INVITED PAPER *Special Section on Emerging Communication Technologies in Conjunction with Main Topics of ICETC 2023*

Wideband Interference Suppression for Automotive mmWave CS Radar: From Algorithm-Based to Learning-Based Approaches

Xiaoyan WANG[†a)], ***Member***, **Ryoto KOIZUMI**[†], ***Nonmember***, **Masahiro UMEHIRA**[††], ***Fellow***, **Ran SUN**[†], ***and*** **Shigeki TAKEDA**[†], ***Members***

SUMMARY In recent times, there has been a significant focus on the development of automotive high-resolution 77 GHz CS (Chirp Sequence) radar, a technology essential for autonomous driving. However, with the increasing popularity of vehicle-mounted CS radars, the issue of intensive inter-radar wideband interference has emerged as a significant concern, leading to undesirable missed targe detection. To solve this problem, various algorithm and learning based approaches have been proposed for wideband interference suppression. In this study, we begin by conducting extensive simulations to assess the SINR (Signal to Interference plus Noise Ratio) and execution time of these approaches in highly demanding scenarios involving up to 7 interfering radars. Subsequently, to validate these approaches could generalize to real data, we perform comprehensive experiments on inter-radar interference using multiple 77 GHz MIMO (Multiple-Input and Multiple-output) CS radars. The collected real-world interference data is then utilized to validate the generalization capacity of these approaches in terms of SINR, missed detection rate, and false detection rate.

key words: *wideband inter-radar interference, algorithm-based approach, learning-based approach, experimental evaluations*

1. Introduction

Currently, there is a growing fascination with autonomous driving technology, spurred by the aim of alleviating traffic congestion and providing highly convenient modes of transportation [1]. The success of autonomous driving heavily relies on the efficacy of onboard sensing techniques to perceive the surrounding environment. Unlike cameras [2] and LiDAR (Light Detection and Ranging) [3], radar systems offer a cost-effective solution and demonstrate robustness against harsh weather conditions such as wind, rain, and fog [4]. Among radar systems, Chirp Sequence (CS) radar stands out as a promising cornerstone due to its capability to simultaneously detect distances and relative velocities of multiple targets [5]. To accurately distinguish pedestrians and motorcycles, a distance resolution of around 0.2 meters is required, necessitating a frequency bandwidth of 3 GHz [6]. Consequently, it is anticipated that high-resolution radars operating in millimeter Wave (mmWave) frequency band will see widespread adoption in the future. As a result, radar interference stemming from this dense deployment of numerous radars is expected to emerge as a significant concern [7].

Inter-radar interference [8] could be categorized into two distinct types: narrowband (or coherent) interference [9], which induces spurious peaks in the frequency spectrum, resulting in false detections of non-existent targets (referred to as ghost targets); and wideband (or non-coherent) interference [10], which elevates the noise level in the frequency spectrum, leading to missed detections of targets. Wideband interference is notably more prevalent compared to narrowband interference. This study concentrates on suppressing wideband interference.

In recent years, extensive researches have been conducted on wideband interference suppression techniques, encompassing both algorithm-based and learning-based approaches. Algorithm-based methods typically utilize a threshold in the time domain to identify interference samples, whereas learning-based approaches reconstruct interference-suppressed time samples without relying on predefined thresholds. Among these techniques, the zero suppression method [11] stands out as a straightforward yet widely employed approach, where a threshold is calculated to detect interference and subsequently suppress interfered samples by setting them to zero. Iterative interference suppression approaches have been introduced to adaptively control the interference detection threshold based on the characteristics of the received beat signal [12]–[14]. However, it has been observed that zero and iterative suppression approaches may encounter challenges, particularly when the duration of interference is prolonged. To address this limitation, an advanced envelope detection and sorting approach has been proposed [15]. Additionally, beyond time-domain methods, spatial-domain detector designs have been proposed to mitigate mutual interference among automotive radars [16]. Furthermore, research has delved into investigating adaptive beamforming techniques, such as the Least Mean Squares (LMS) algorithm-based approach [17], to effectively suppress interference.

Recently, learning-based techniques have emerged as promising solutions, showing remarkable performance. Specifically, [18] explored a Convolutional Neural Network (CNN)-based method tailored for mitigating inter-radar interference. Similarly, [19] introduced an interference mitigation method for CS radars by employing signal reconstruction grounded on autoregressive (AR) models. Additionally, in [20], a Fully Convolutional Network (FCN) was put forward to address interference and noise in the time-frequency spec-

Manuscript received February 17, 2024.
Manuscript revised May 17, 2024.
Manuscript publicized August 22, 2024.

[†]Graduate School of Science and Engineering, Ibaraki University, Hitachi-shi, 316-8511 Japan.
[††]Department of Electronics and Communication Technology, Nanzan University, Nagoya-shi, 466-8637 Japan.
a) E-mail: xiaoyan.wang.shawn@vc.ibaraki.ac.jp (Corresponding author)

DOI: 10.23919/transcom.2024CEI0002

trum. Moreover, [21], [22] presented and assessed methods utilizing Recurrent Neural Networks (RNNs) for automotive radar signal interference mitigation.

In this paper, we delve into the investigation of three algorithm-based approaches (i.e., zero suppression [11], iterative suppression [12]–[14], envelope suppression [15]) and one learning-based approach (i.e. RNN suppression [21], [22]), evaluating their efficacy through both simulations and practical experiments. It is reported that these approaches have promising results by simulations with up to 4 interfering radars in their respective papers. However, there is still concerns regarding their performance in extra-dense interference scenario and the generalization capacity on real-world data. To this end, in this paper, initially, we gauge their interference suppression capabilities in terms of Signal to Interference plus Noise Ratio (SINR) and execution time via simulations conducted in highly demanding environments featuring up to 7 interfering radars. Subsequently, we undertake comprehensive experiments utilizing multiple 77 GHz Multiple-Input and Multiple-Output (MIMO) CS radars to capture real-world data across various inter-radar interference scenarios. The collected real data is then utilized to validate the generalization capacity of these approaches, considering metrics including SINR, missed detection rate, and false detection rate.

2. Inter-Radar Wideband Interference

2.1 CS Radar

A sequence of chirp signals modulated by a sawtooth waveform are transmitted and reflected off the target. These signals are subsequently multiplied by a mixer and filtered through a Low Pass Filter (LPF) to yield the beat signal, which is proportional to the delay between transmitted and received signals. Following this, the signal undergoes Analog-Digital Conversion (ADC), and Fast Fourier Transform (FFT) is applied. Target detection is then performed in the obtained frequency spectrum, typically employing peak detection algorithms like the Constant False Alarm Rate (CFAR) method. Utilizing the beat frequency at the detected peak, the distance and relative velocity of the target can be determined.

2.2 Inter-Radar Wideband Interference

In the presense of inter-radar interference, the time domain received signal $r(i)$ is expressed as the following equation, which consists of the target echo signal $e(i)$, the interfering signal $int(i)$ and the noise signal $n(i)$.

$$r(i) = e(i) + int(i) + n(i) \tag{1}$$

The echo signal $e(i)$ from the target is expressed as follows.

$$e(i) = A\cos\left(2\pi\left(\frac{2f_cR}{c} + \left(\frac{2f_cv}{c} + \frac{2\Delta fR}{Tc}\right)i\right)\right), \tag{2}$$

where c is the speed of light, A, f_c, Δf, T are the signal amplitude, center frequency, bandwidth and chirp period, R, v are the distance and relative velocity of the target, respectively. The interfering signal $int(i)$ could be expressed as follows.

$$int(i) = A_{int}\cos\left(2\pi\left((f_{int} - f_c)\,i + \frac{1}{2}\left(\frac{\Delta f_{int}}{T_{int}} - \frac{\Delta f}{T}\right)i^2 + \frac{\Delta f_{int}}{T_{int}}\tau i\right) + \phi\right), \tag{3}$$

where A_{int}, f_{int}, Δf_{int}, T_{int} are the interfering signal's ampulitude, center frequency, bandwidth and chirp period, τ and ϕ are the time delay and phase difference between the transmitted and interfering chirps, respectively.

Inter-radar interference could be divided into two categories, i.e., narrowband interference and wideband interference. Narrowband interference occurs when the transmitted signal's chirp rate ($\frac{\Delta f}{T}$) is the same as the interfering signal's chirp rate ($\frac{\Delta f_{int}}{T_{int}}$), and the time delay ($\phi$) between the transmitted and interfering chirps is very small. It will generate a fake peak in the frequency spectrum, and thus lead to false detection of the target. Narrowband interference suppression methods [9] are out of the scope of this research.

Wideband interference occurs when $\frac{\Delta f}{T}$ differs from $\frac{\Delta f_{int}}{T_{int}}$. As depicted in Fig. 1, we can notice that alongside the beat frequency of the echo signal from the target, an additional beat frequency originating from the interfering radar is evident which is shown in red color. Consequently, when the beat frequency of the interfering radar falls below the passband of the LPF, an interfering beat signal emerges, as indicated by the green circle in Fig. 1. These interfered

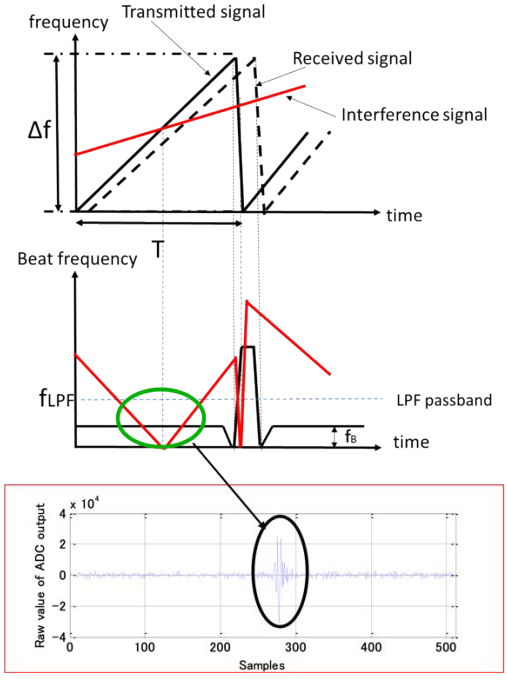

Fig. 1 Inter-radar wideband interference.

samples could be detected by using a threshold in the time domain, since the power of the interfering signal given in Eq. (3) is generally much higher than that of the echo signal of the target given in Eq. (2). This interference leads to an elevated noise level across the frequency spectrum, thereby increasing the missed detection rate of the target.

3. Wideband Interference Suppression Approaches

In this section, we briefly introduce four representative wideband interference suppression approaches, i.e., zero suppression, iterative suppression, envelope suppression and RNN suppression approaches.

3.1 Zero Suppression Approach [11]

Zero suppression approach is a straightforward yet widely utilized method for suppressing inter-radar interference. This approach operates by employing a threshold in time domain to identify interference samples and suppress them to zero. More precisely, a threshold R_{th} is established by using the weighted average beat signal samples $r(i)$ as follows.

$$R_{th} = k\frac{1}{N}\sum_{i=1}^{N}|r(i)|, \tag{4}$$

where N is the number of samples, k is a parameter to adjust the threshold. In the interfered beat signal, samples with an absolute value greater than the threshold, i.e., $|r(i)| > R_{th}$, are identified as interference, and their values are then set to 0. However, obviously this method encounters difficulty in effectively handling different types of interference by using the same threshold R_{th}.

3.2 Iterative Suppression Approach [12]–[14]

In iterative suppression approach, thresholds to detect and suppress the interference are calculated iteratively. An initial threshold R_{th} is set similar as that in zero suppression approach by using Eq. (4) and all the samples that exceed this threshold are set to zero initially. Next, for the unsuppressed beat signal, a new threshold R'_{th} is calculated again, and the samples that exceed the new threshold are set to zero similarly. This process repeats until the difference between R_{th} and R'_{th} satisfies a predetermined convergence criterion. This approach is capable of adaptively setting the threshold according to different interference power. However, it may fail when the interference duration is considerable long, as in such cases, the initial threshold may be higher than the interference level and thus the interference samples may not be detected at all. The flow chart of the iterative suppression approach is illustrated in Fig. 2.

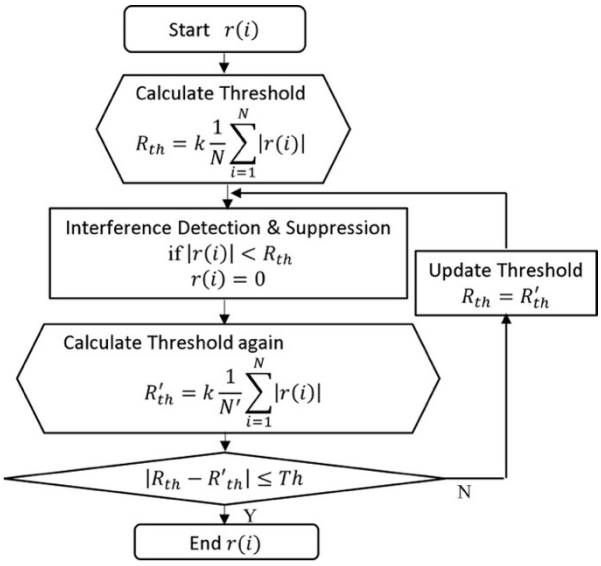

Fig. 2 Iterative suppression approach.

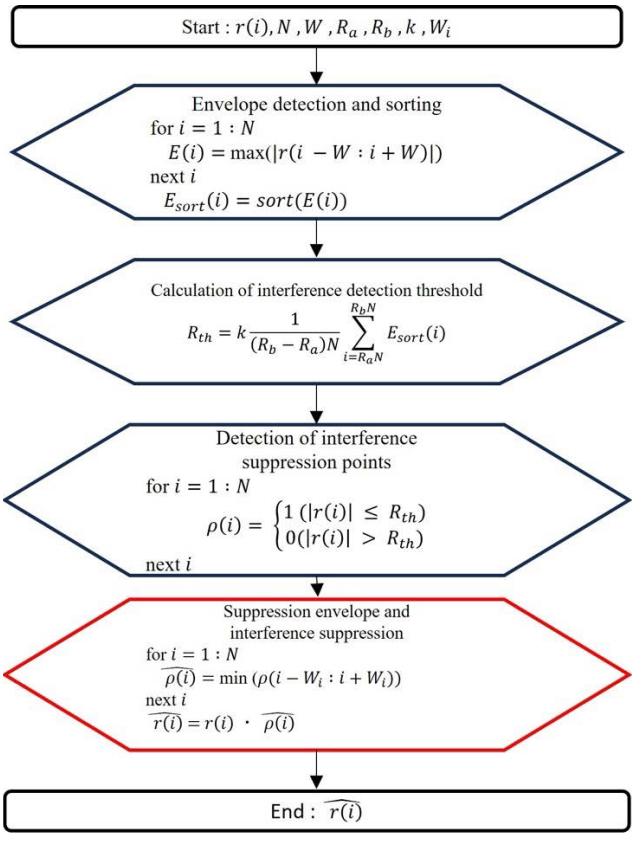

Fig. 3 Envelope suppression approach.

3.3 Envelope Suppression Approach [15]

The previously mentioned problem can be resolved by establishing a threshold with desired signal only. To this end, envelope suppression approach uses envelope detection and sorting to extract the desired signal from the interfered received signal and calculate the threshold. Figure 3 illustrates its process, which can be briefly summarized as follows. Initially, the envelope data $E(i)$ is derived from the beat signal $r(i)$ consisting of N time samples. It employs a sliding win-

dow with a width of $2W + 1$ applied to the absolute values $|r(i)|$ $(i = 1, 2, \ldots, N)$ of the beat signal, calculating the maximum value within the window. Subsequently, the envelope $E(i)$ is sorted in ascending order, and an interference detection threshold R_{th} is established by using parameters k, R_a and R_b $(0 < R_a < R_b < 1)$.

Consequently, samples with $|r(i)| > R_{th}$ are identified as interference and are suppressed to zero. Lastly, the suppression envelope $\widehat{\rho(i)}$ is calculated for each sample i by using a sliding window W_i, facilitating the elimination of residual interference noise after zero suppression. Notice that the last step in this approach is optional, which is marked as red in Fig. 3. Compared with zero suppression and iterative suppression approaches, the envelope suppression approach is capable of detecting and suppressing the wideband interference in severe conditions when the number of interference is large or the interference duration is long.

3.4 RNN Suppression Approach [21], [22]

All the aforementioned algorithm-based interference suppression approaches rely on an interference detection threshold, which then is used to suppress the interfered samples into zero. On the contrary, the RNN approach is threshold-free, and tries to reconstruct the interfered samples instead of setting them to zero. RNN is a neural networks class characterized by cyclic connections between neurons, making it ideal for processing and learning from sequential or time-series data. In the RNN suppression approach, the input $r(i)$ is the beat signal with interference, and the label $\widehat{r(i)}$ is the beat signal without interference. The input and label could be either generated in simulation or obtained in experiment in pairs. Specifically, each pair of input and label has the same target condition (e.g., the number of targets, target distance, target velocity, etc.) and radar signal parameters (e.g. center frequency, chirp period, bandwidth, etc.). The goal of the learning process is to minimize the loss function L, which is defined as the Mean Squared Error (MSE) between the output $r'(i)$ and label $\widehat{r(i)}$. After the training process converges, the RNN model's output $r'(i)$ will be the beat signal in which the interference has been suppressed.

4. Simulation Evaluation

In this section, we assess the effectiveness of conventional zero suppression, iterative suppression, envelope suppression, and RNN suppression approaches through simulations conducted in an extremely demanding scenario involving up to 7 interfering radars. The radar parameters are randomly generated from the ranges given by Table 1, which are similar to most of the related work that uses fast chirp CS radars [7]–[15]. The RNN model is trained using 50 scenarios, each scenario consists of beat signal with 75 chirps, thus the total training data is 3750. It is tested by another 20 scenarios that have never been used in the training. The optimizer used is Adam, and the loss function employed is MSE. The parameter configurations for these four approaches are outlined in Table 2, respectively. The parameter k in the zero suppression is a typical setting, by which the impulse-like interference could be successively detected. The parameter settings for iterative and envelope suppression approaches are based on their respective papers [12], [15], which achieve the best performance. Obviously, larger k results in better false detection rate but worse miss detection rate, and vice versa. The parameter settings for RNN suppression are based on [22]. Notice that there is a tradeoff between the SINR performance and inference time depending on the RNN model size. The specific discussions on this tradeoff could be found at [23].

Table 1 Radar parameter settings.

Parameters	Values
Center frequency	76~78 [GHz]
Distance	1~130 [m]
Velocity	1~50 [km/h]
Chirp period	20~40 [μs]
Sweep bandwidth	100~200 [MHz]
Number of targets	1~2
Number of interferences	1~7

Table 2 Parameter settings for different approaches.

Approach	Parameters	Values
Zero suppression	k	1
Iterative suppression	Window W	24
	k	5
	Threshold Th	0
Envelope suppression	Window W	32
	R_a~R_b	0.25~0.5
	k	1.5
	Window W_i	2
RNN suppression	Learning rate	0.001
	Epoch	1000
	Hidden state size	100
	Number of layers	3
	Batch size	128

Figures 4 and 5 depict the time waveform and frequency spectrum in a scenario featuring 1 interference radar. Specifically, in Figs. 4(a)–(f), the waveforms are presented without interference, with interference but without suppression, with zero suppression, with iterative suppression, with envelope suppression, and with RNN suppression, respectively. It can be observed that while zero suppression fails to completely identify interfered samples, both iterative suppression and envelope suppression effectively detect and suppress interfered samples to zero. In contrast, the RNN suppression approach yields a suppressed waveform closely resembling the one without interference. Upon performing FFT, the corresponding frequency spectrum are obtained and presented in Figs. 5(a)–(f). It is evident that all four approaches successfully reduce the noise level while maintaining peak power.

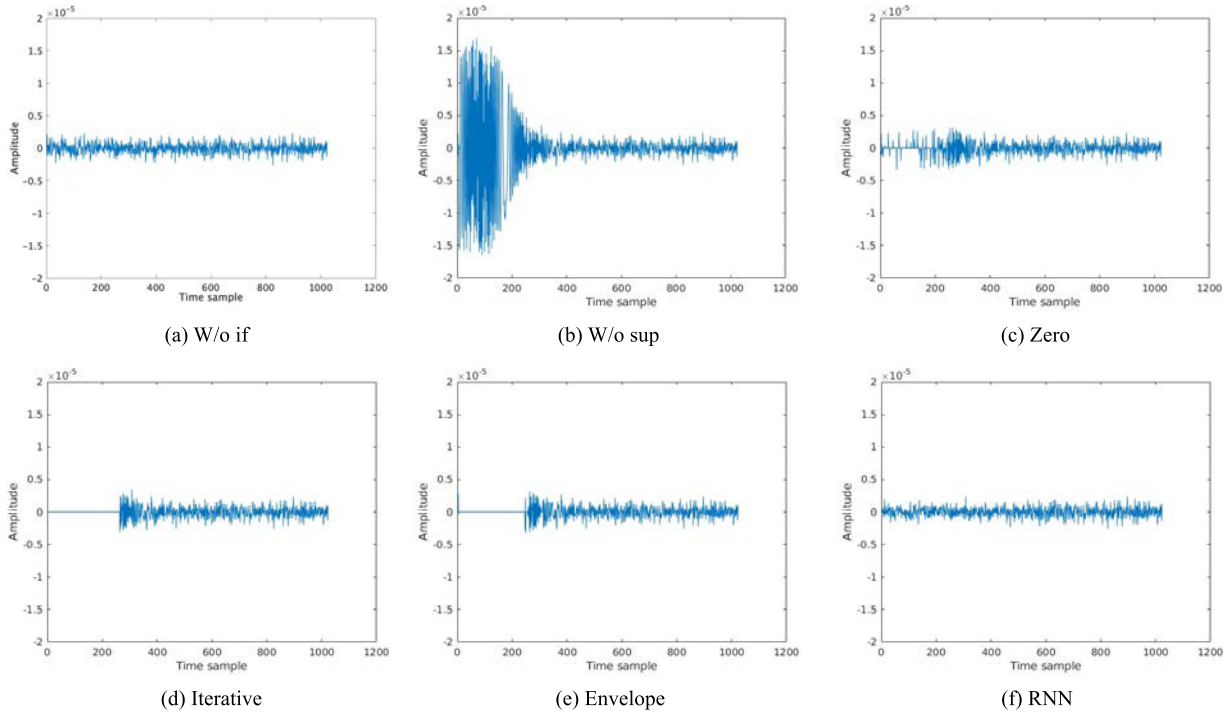

(a) W/o if (b) W/o sup (c) Zero

(d) Iterative (e) Envelope (f) RNN

Fig. 4 Time waveform (1 interfering radar).

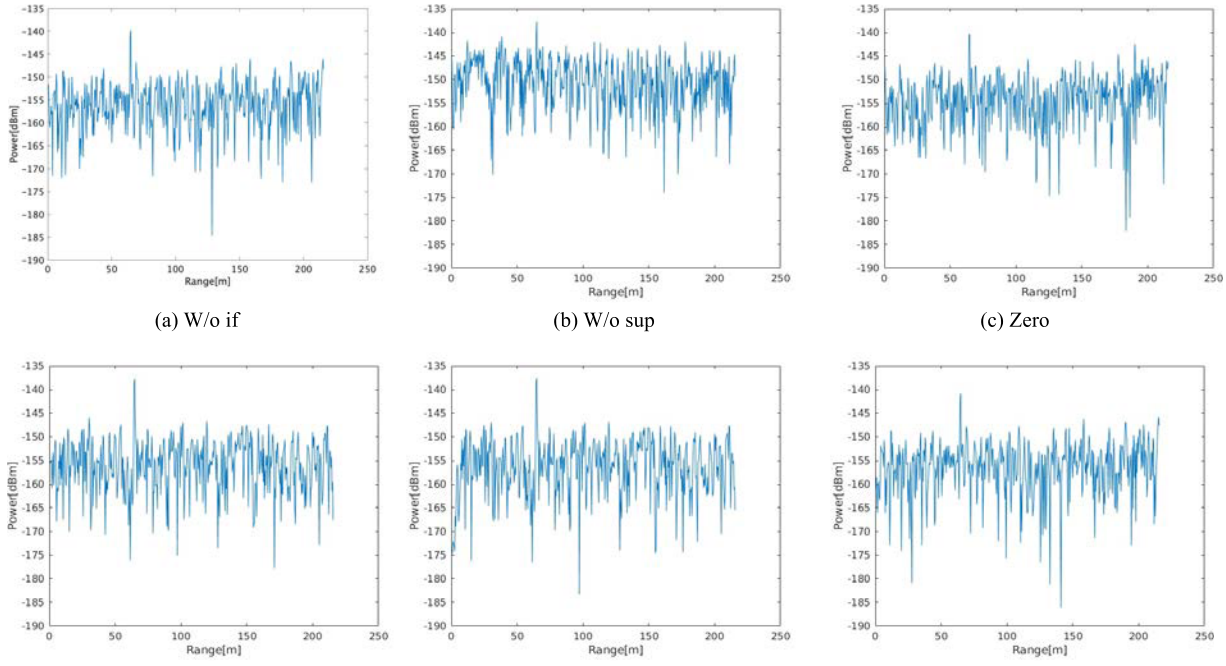

(a) W/o if (b) W/o sup (c) Zero

(d) Iterative (e) Envelope (f) RNN

Fig. 5 Frequency spectrum (1 interfering radar).

To assess the achieved SINR, we average the results from 10 different scenarios with 1 interfering radar. As depicted in Fig. 6, the RNN suppression exhibits marginally superior performance compared to algorithm-based approaches on average. Additionally, the envelope suppression approach outperforms the iterative suppression approach slightly, especially in low SINR scenarios.

Figures 7(a)–(f) depict the frequency spectrum in a scenario involving 7 interfering radars. From Fig. 7(b), it is evident that the target around 70 m is entirely obscured by noise. In this exceptionally challenging scenario, the conventional zero suppression method fails to diminish the noise level, and

the peak cannot be reliably detected by the CFAR method. Conversely, iterative suppression, envelope suppression, and RNN suppression manage to reduce the noise level to some degree, however, none of them can consistently maintain peak power. As illustrated in Fig. 8, it becomes apparent that the RNN suppression approach outperforms the algorithm-based methods, demonstrating the smallest deviation from the results obtained without interference. The performance enhancement of RNN approach comes with the trade-off of requiring a pre-training process with the clean beat signal, unlike algorithm-based approaches which do not necessitate it. Furthermore, the iterative suppression method outperforms the envelope suppression approach in scenarios with high SINR, but exhibits inferior performance in scenarios with low SINR.

Finally, we evaluate the execution time of one chirp for these inter-radar interference suppression approaches. The CPU we utilized is an intel Core i9-12900H, and the GPU is an Nvidia RTX A5500 Laptop. The evaluation results are summarized in Table 3. It is obvious that compared with algorithm-based approaches, the RNN suppression approaches has much longer inference time. Noted that the pre-learning is required for RNN suppression approach, which lasts 14.51 hours for a training dataset with 50 scenarios.

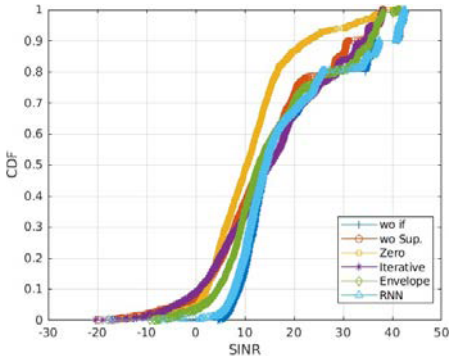

Fig. 6 SINR in scenario with 1 interfering radar (simulation data).

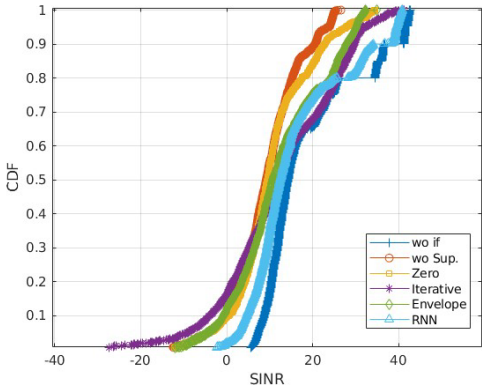

Fig. 8 SINR in scenario with 7 interfering radars (simulation data).

Table 3 Execution time comparison.

Approaches	Execution time [ms]
Zero	0.0176
Iterative	0.0212
Envelope	0.0429
RNN (w/ GPU)	32.27
RNN (w/ CPU)	327.6

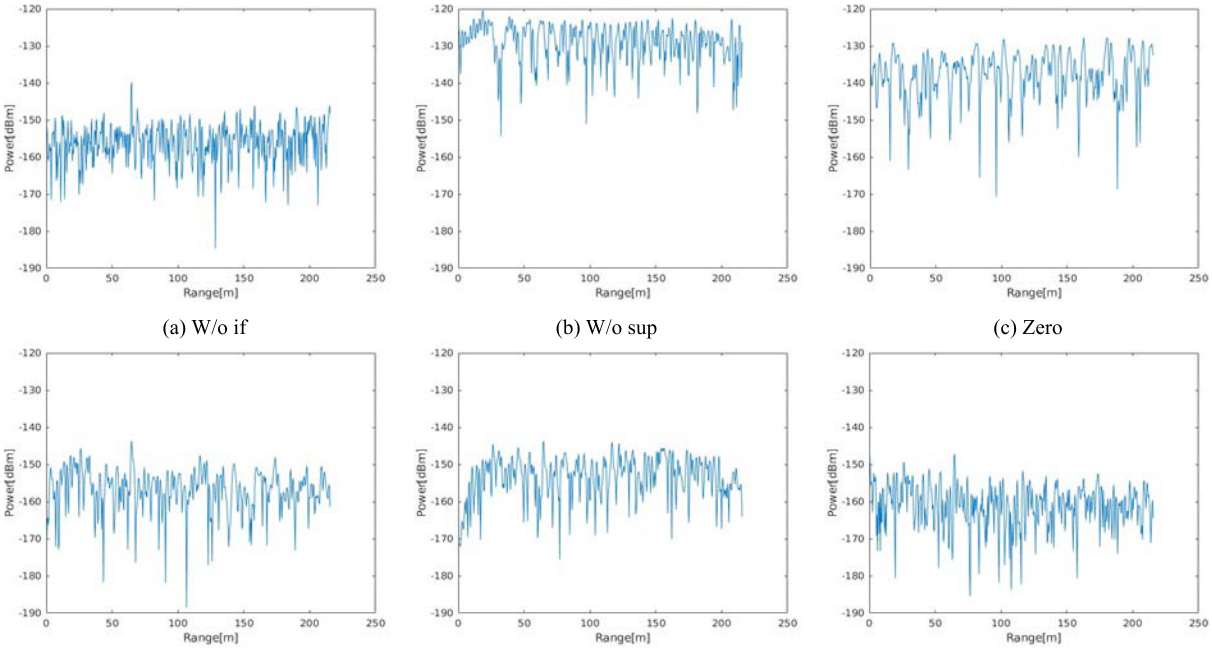

(a) W/o if (b) W/o sup (c) Zero

(d) Iterative (e) Envelope (f) RNN

Fig. 7 Frequency spectrum (7 interfering radars).

Reducing the inference time of RNN approach will be one of our future work.

In conclusion, based on our extensive simulation results, we find that iterative suppression, envelope suppression, and RNN suppression approaches are all effective in suppressing inter-radar interference in highly challenging scenarios involving up to 7 interfering radars.

5. Inter-Radar Interference Experiment and Evaluation

5.1 Experimental Scenario and Settings

To verify the real-world efficacy of these inter-radar interference suppression approaches, we conducted extensive inter-radar experiments utilizing 77 GHz MIMO CS radars. As depicted in Fig. 9(a), these experiments were carried out at a stadium in Nanzan University, Japan. The experimental setup is illustrated in Fig. 9(b). The number of targets was 1 and 2, and the distance of them were ranging from 5 m to 20 m. While the number of interfering radars was 1 to 4, and their distances were ranging from 4 m to 5 m. 2×4 MIMO CS radars equipped with 2 transmitting antennas and 4 receiving antennas were utilized. The chirp rates and sweep bandwidth were set at 25 µs, 50 µs and 1 GHz, 2 GHz, respectively. A trigger pulse generator was employed to ensure wideband interference occurrence by controlling the timing of transmitting signals. Each radar was connected to a notebook via a PoE interface, facilitating the observation, recording, and processing of measurement data. Noted that

(a) Experimental scene

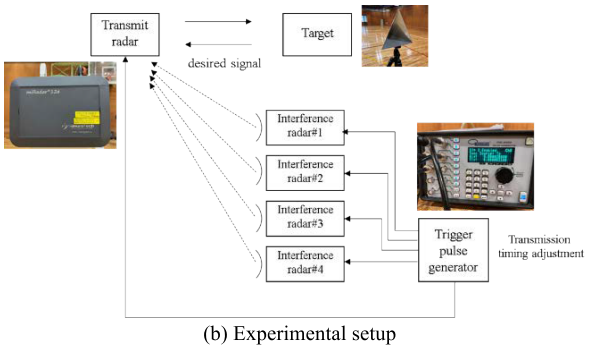

(b) Experimental setup

Fig. 9 Inter-radar interference experiment.

the input data and labels are recorded in pairs during the experiment, corresponding to scenarios with and without radar interference.

We utilize the collected real inter-radar interference data to assess the generalization capacity of the zero suppression, iterative suppression, envelope suppression, and RNN suppression approaches on real data. Regarding the RNN suppression approach, we develop three distinct models: one trained using simulation data, another trained using experimental data, and a third model pre-trained using simulation data and subsequently fine-tuned using experimental data. The models trained on both simulation and experimental data have a training dataset size of 1600 samples (50 scenarios with 32 chirps each). The fine-tuning model is first trained using simulation data from 50 scenarios, and then further refined using experimental data from 10 scenarios. All the approaches are tested by 10 scenarios, which are never used in the training.

5.2 Evaluation Results

Figure 10 depicts the time waveforms of a scenario involving 4 interfering radars, with the target positioned at 10 m. Specifically, Figs. 10(a)–(f) illustrate the time waveforms without interference, with interference but without suppression, with zero suppression, with iterative suppression, with envelope suppression, with RNN suppression using the simulation model, with RNN suppression using the experimental model, and with RNN suppression by fine-tuning, respectively. It is observed that all three algorithm-based approaches fail to perfectly identify the interfered samples, likely due to the establishment of a threshold that is too large owing to the prolonged duration of interference. Similarly, the RNN suppression using the simulation model is unable to completely suppress the interference, while the RNN suppression by fine-tuning tends to degrade the desired signal. Among these methods, the RNN suppression using the experimental model demonstrates the best performance, generating an interference-suppressed beat signal that closely resembles the signal without interference.

Figures 11(a)–(f) display the corresponding frequency spectrum. It is evident that the interference is effectively suppressed, leading to an improvement in SINR when employing RNN suppression with the experimental model. The peak power remains at −60 dBm, with the noise level around the peak reduced to approximately −85 dBm. In contrast, the other approaches exhibit limited efficacy, with no significant improvement in SINR observed. Notably, the RNN suppression by fine-tuning performs poorly in this scenario, as the peak at 10 m can hardly be detected due to the damage of the desired signal.

We then assess the Cumulative Distribution Function (CDF) of the SINR for all approaches across scenarios involving interfering radars ranging from 1 to 4. To calculate SINR, we first detect a reference peak $\hat{p}$ in the frequency spectrum without interference. Subsequently, in the frequency spectrum with interference under the same condi-

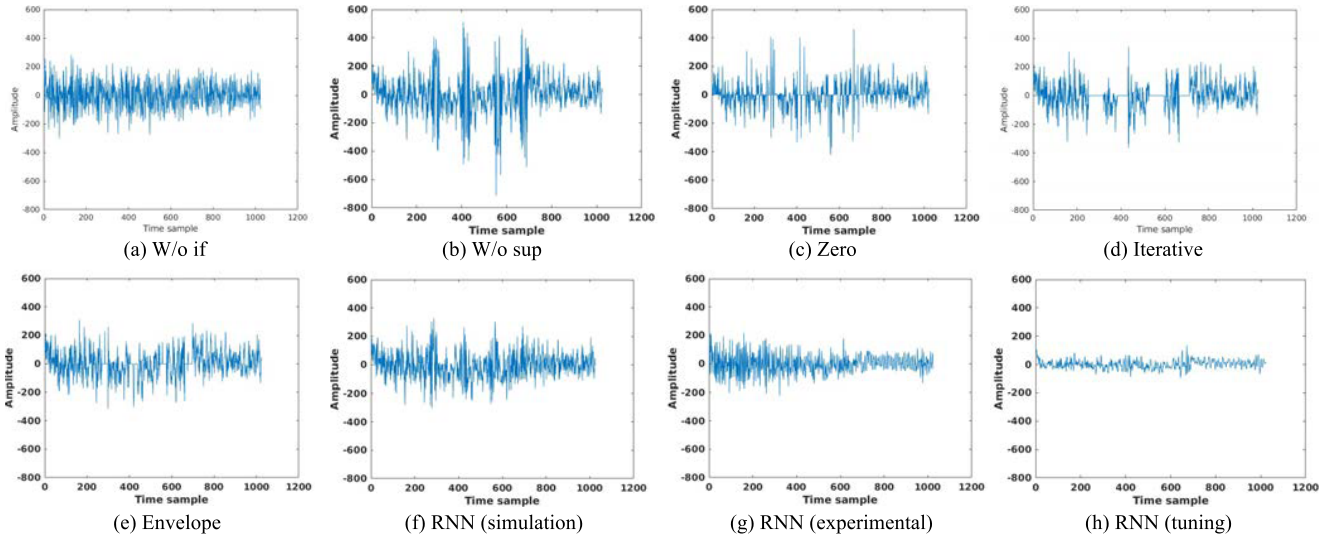

(a) W/o if (b) W/o sup (c) Zero (d) Iterative

(e) Envelope (f) RNN (simulation) (g) RNN (experimental) (h) RNN (tuning)

Fig. 10 Time waveform of the experimental data (4 interfering radars).

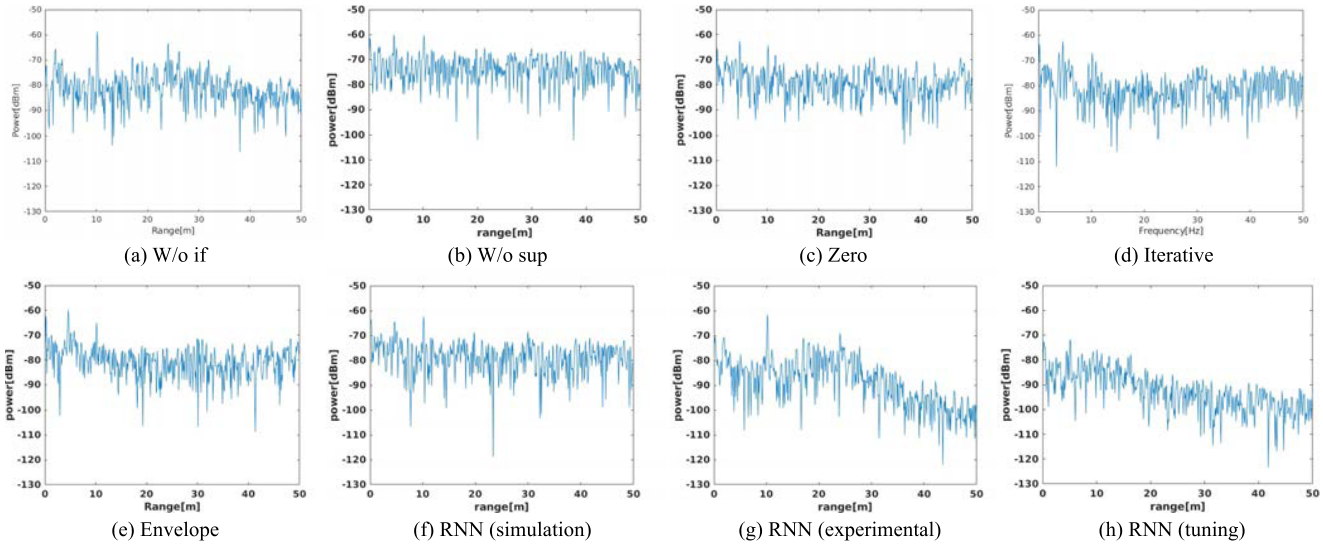

(a) W/o if (b) W/o sup (c) Zero (d) Iterative

(e) Envelope (f) RNN (simulation) (g) RNN (experimental) (h) RNN (tuning)

Fig. 11 Frequency spectrum of the experimental data (4 interfering radars).

tions, we identify a peak p around the reference peak. Next, we regard 80 samples around the peak p as the noise level and use the power of p and noise level to calculate the SINR. This calculation is repeated for all chirps, allowing us to compute the average achieved SINR. As depicted in Fig. 12, the RNN suppression approaches outperform the algorithm-based approaches on average. Specifically, the RNN model trained using experimental data exhibits the highest performance, maintaining a minimal gap between the results obtained without interference. Conversely, the model trained using simulation data demonstrates relatively lower performance. Notably, the conventional zero suppression approach even exhibits worse performance on average than the results obtained without suppression during this evaluation using real-world data.

Finally, we evaluate the missed detection rates and false detection rates for all approaches across scenarios involving

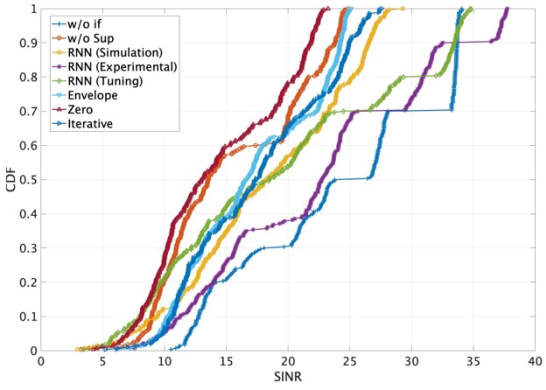

Fig. 12 SINR for scenarios with 1–4 interfering radars (experimental data).

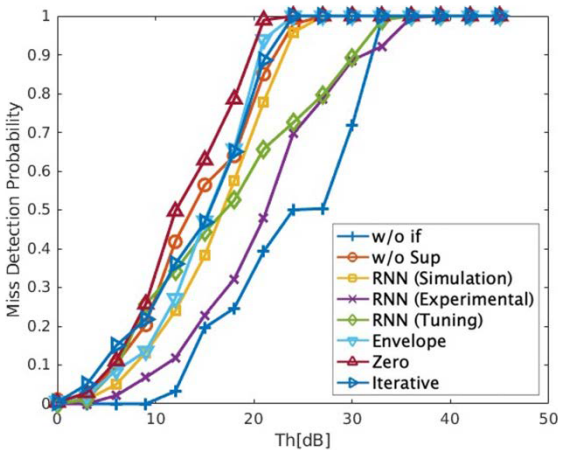

Fig. 13 Missed detection rate (experimental data).

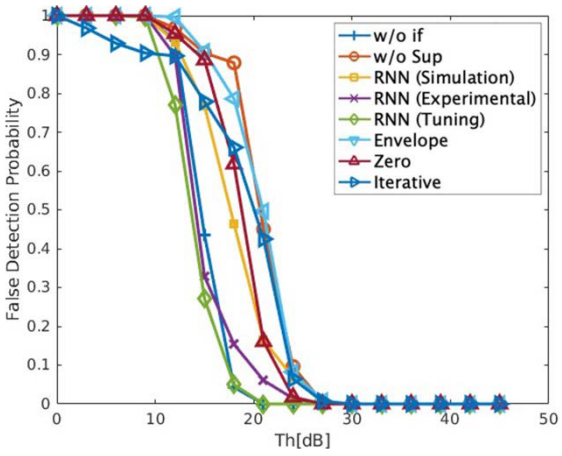

Fig. 14 False detection rate (experimental data).

interfering radars ranging from 1 to 4. The peak detection relies on CFAR method, and its procedure is outlined as follows. For each sample i in the beat signal, an (e) Envelope (f) RNN (simulation) (g) RNN (experimental) (h) RNN (tuning) average noise level $n(i)$ is calculated with a sliding window of size 24. An interference detection threshold for sample i is then determined by adding a parameter Th to $n(i)$. If sample i exceeds this threshold and is within a small range of the reference peak $\hat{p}$ (i.e., 3 samples before and after), the target is considered correctly detected. Consequently, the missed detection rate is derived by $(1 - N_T/N)$, where N_T is the number of chirps with correctly detected peaks, and N is the total number of chirps. On the other hand, if at least one sample exceeds the threshold and lies outside the small range of reference peak $\hat{p}$, it is deemed a false detection. The evaluation results for missed detection rates and false detection rates are shown in Figs. 13 and 14, respectively. As the threshold parameter Th increases, the false detection rate decreases while the missed detection rate increases. Hence, it can be inferred that there exists a trade-off relationship between them, and an optimal Th exists to minimize their sum. Moreover, across all cases, the RNN suppression approaches, particularly the models utilizing experimental data and fine-tuning, demonstrate superior performance.

6. Conclusion

This paper introduces three algorithm-based and one learning-based approaches for inter-radar wideband interference suppression, evaluating their performance in both simulated and real-world settings. Through extensive simulation, we showed that in a highly challenging scenario with 7 interfering radars, iterative suppression, envelope suppression, and RNN suppression managed to reduce the noise level to some extent. However, none of them could consistently maintain peak power. On average, the RNN suppression approach performed the best, showing the smallest deviation from results obtained without interference.

Moreover, we carried out comprehensive inter-radar interference experiments using 77 GHz MIMO CS radars to gather real-world data. Performance evaluations, including comparisons in terms of SINR, missed detection rate, and false detection rate, were conducted for all approaches utilizing this real-world data. Moving forward, our focus will be on evaluating the trade-off between achieved SINR and inference time, as well as enhancing model accuracy by optimizing the architecture and hyperparameters.

Acknowledgements

This research and development work was supported by the MIC/SCOPE ## JP225003006.

References

[1] X. Cheng, R. Zhang, and L. Yang, "Wireless toward the era of intelligent vehicles," IEEE Internet Things J., vol.6, no.1, pp.188–202, Feb. 2019.
[2] V.R. Kumar, C. Eising, C. Witt, and S.K. Yogamani, "Surround-view fisheye camera perception for automated driving: Overview, survey & challenges," IEEE Trans. Intelligent Transp. Syst., vol.24, no.4, pp.3638–3659, April 2023.
[3] R. Roriz, J. Cabral, and T. Gomes, "Automotive LiDAR technology: A survey," IEEE Trans. Intell. Transp. Syst., vol.23, no.7, pp.6282–6297, July 2022.
[4] A. Venon, Y. Dupuis, P. Vasseur, and P. Merriaux, "Millimeter wave FMCW radars for perception, recognition and localization in automotive applications: A survey," IEEE Trans. Intell. Veh., vol.7, no.3, pp.533–555, Sept. 2022.
[5] C. Waldschmidt, J. Hasch, and W. Menzel, "Automotive radar — From first efforts to future systems," IEEE J. Microw., vol.1, no.1, pp.135–148, Jan. 2021.
[6] R. Sun, J. Sakai, K. Suzuki, J. Zheng, S. Takeda, M. Umehira, X. Wang, and H. Kuroda, "Antenna element space interference cancelling radar for angle estimations of multiple targets," IEEE Access, vol.9, pp.72547–72555, 2021.
[7] M. Umehira, Y. Watabe, X. Wang, S. Takeda, and H. Kuroda, "Inter-radar interference in automotive FMCW radars and its mitigation challenges," Proc. IEEE International Symposium on Radio-Frequency Integration Technology (RFIT 2020), Sept. 2020.
[8] S. Rao and A.V. Mani, "Interference characterization in FMCW radars," Proc. IEEE Radar Conference (RadarConf20), Florence, Italy, pp.1–6, 2020.
[9] D. Ammen, M. Umehira, X. Wang, S. Takeda, and H. Kuroda,

"A ghost target suppression technique using interference replica for automotive FMCW radars," Proc. IEEE Radar Conference (RadarConf20), Florence, Italy, pp.1–5, 2020.

[10] Y. Makino, T. Nozawa, M. Umehira, X. Wang, S. Takeda, and H. Kuroda, "Inter-radar interference analysis of FMCW radars with different chirp rates," J. Engineering, vol.2019, no.19, pp.5634–5638, Oct. 2019.

[11] G.M. Brooker, "Mutual interference of millimeter-wave radar systems," IEEE Trans. Electromagn. Compat., vol.49, no.1, pp.170–181, Feb. 2007.

[12] M. Umehira, T. Nozawa, Y. Makino, X. Wang, S. Takeda, and H. Kuroda, "A novel iterative inter-radar interference reduction scheme for densely deployed automotive FMCW radars," Proc. 19th International Radar Symposium (IRS), Bonn, Germany, pp.1–10, 2018.

[13] T. Okuda, Y. Makino, M. Umehira, X. Wang, S. Takeda, and H. Kuroda, "Prototype development and experimental performance evaluation of FMCW radar using iterative interference suppression technique," Proc. International Radar Conference (RADAR), Toulon, France, pp.1–6, 2019.

[14] M. Umehira, T. Okuda, X. Wang, S. Takeda, and H. Kuroda, "An adaptive interference detection and suppression scheme using iterative processing for automotive FMCW radars," Proc. IEEE Radar Conference (RadarConf20), Florence, Italy, pp.1–5, 2020.

[15] T. Shimura, M. Umehira, Y. Watanabe, X. Wang, and S. Takeda, "An advanced wideband interference suppression technique using envelope detection and sorting for automotive FMCW radar," Proc. IEEE Radar Conference (RadarConf22), New York City, NY, USA, pp.1–6, 2022.

[16] S. Jin, P. Wang, P. Boufounos, R. Takahashi, and S. Roy, "Spatial-domain object detection under MIMO-FMCW automotive radar interference," Proc. IEEE International Conference on Acoustics, Speech and Signal Processing (ICASSP), Rhodes Island, Greece, pp.1–5, 2023.

[17] M. Rameez, M. Dahl, and M.I. Pettersson, "Experimental evaluation of adaptive beamforming for automotive radar interference suppression," Proc. IEEE Radio and Wireless Symposium (RWS), San Antonio, TX, USA, pp.183–186, 2020.

[18] J. Rock, M. Toth, P. Meissner, and F. Pernkopf, "Deep interference mitigation and denoising of real-world FMCW radar signals," Proc. IEEE Int. Radar Conf. (RADAR), pp.624–629, April 2020.

[19] M. Rameez, M. Dahl, and M.I. Petterson, "Autoregressive model-based signal reconstruction for automotive radar interference mitigation," IEEE Sensors J., vol.21, no.5, pp.6575–6586, March 2021.

[20] R. Li, J. Wang, Y. He, Y. Yang, and Y. Lang, "Deep learning for interference mitigation in time-frequency maps of FMCW radars," Proc. CIE International Conference on Radar (Radar), Haikou, Hainan, China, pp.1883–1886, 2021.

[21] J. Mun, S. Ha, and J. Lee, "Automotive radar signal interference mitigation using RNN with self attention," Proc. IEEE Int. Conf. Acoust., Speech Signal Process. (ICASSP), pp.3802–3806, May 2020.

[22] R. Koizumi, X. Wang, M. Umehira, S. Takeda, and R. Sun, "RNN-based interference suppression method for CS radar: Simulation and experimental evaluations," Proc. International Conference on Artificial Intelligence in Information and Communication (ICAIIC), Bali, Indonesia, pp.242–247, 2023.

[23] Y. Suzuki, X. Wang, M. Umehira, R. Sun, and S. Takeda, "Performance and inference time tradeoff for RNN model based wideband inter-radar interference mitigation," Proc. International Conference on Ubiquitous and Future Networks, July 2024.

Xiaoyan Wang received the BE degree from Beihang University, China, and the M.E. and Ph.D. from the University of Tsukuba, Japan. He is currently working as an associate professor with the Graduate School of Science and Engineering at Ibaraki University, Japan. Before that, he worked as an assistant professor at National Institute of Informatics (NII), Japan, from 2013 to 2016. His research interests include networking, wireless communications, cloud computing, big data, security and privacy. He is a member of IEICE and senior member of IEEE.

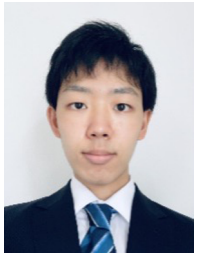

Ryoto Koizumi received the B.E. degree from Ibaraki University in 2022. He is currently a 2nd year master's student in Ibaraki University. His research interest is inter-radar interference suppression technology for in-vehicle radar using machine learning.

Masahiro Umehira received the B.E., M.E. and Ph.D. degrees from Kyoto University, Kyoto, Japan in 1978, 1980 and 2000, respectively. Since joining NTT (Nippon Telegraph and Telephone Corporation) in 1980, he has been engaged in the research and development of modem and TDMA equipment for satellite communications, TDMA satellite communication systems, broadband wireless access systems for mobile multimedia services and ubiquitous wireless systems. From 1987 to 1988, he was with the Communications Research Center, Department of Communications, Canada, as a visiting scientist. Since 2006, he has been a professor of Ibaraki University, Ibaraki, Japan. His research interest includes broadband wireless access technologies, wireless networking, cognitive radio, future satellite communication systems and wireless-based ubiquitous systems. He received Young engineer award and Achievement award from IEICE in 1987 and 1999, respectively. He also received Education, Culture, Sports, Science and Technology Minister Award in 2001 and TELECOM System Technology Award from the Telecommunications advancement Foundation in 2003. He is a fellow of IEICE and life member of IEEE.

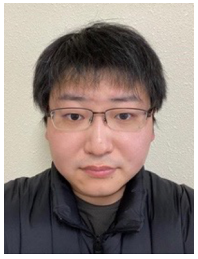

Ran Sun received the B.E., M.E., and Ph.D. degrees in computer and information science from Ibaraki University, in 2016, 2017, and 2020, respectively. Since 2020, he has been an Assistant Professor with Ibaraki University. His research interests include optical wireless communication, error correcting codes, the Internet of Things platform, and vehicle-borne radar. He is a member of IEICE.

Shigeki Takeda received his B.E., M.E. and D.E. degrees in electrical and electronic engineering from Tottori University, Tottori, Japan, in 1996, 1998 and 2000, respectively. Since 2000, he has been with Graduate School of Science and Engineering, Ibaraki University, Ibaraki, Japan, where he is currently a professor. His research interests are in RFID tag, MIMO and adaptive array antenna. He is a member of IEICE.